Research Article

Guodong Zeng, Xinfang Ma*, and Yuehao Liu

Characteristics of tight oil reservoirs and their impact on seepage flow from a nonlinear engineering perspective

https://doi.org/10.1515/nleng-2025-0164
received April 30, 2025; accepted June 17, 2025

Abstract: In order to clarify the characteristics of tight oil reservoirs and their impact on seepage, we conducted a comprehensive analysis of the reservoir characteristics of the Chang-7 tight sandstone using advanced equipment such as X-ray diffractometers and high-pressure mercury injection devices from the perspective of nonlinear engineering. We studied the effect of reservoir characteristics on oil and water seepage. The results show that tight cores are mainly quartz arenite and feldspar arenite with high clay mineral content. They have abundant irregular, disconnected pore spaces and micro-fractures, leading to low permeability and poor physical properties. Tight cores are stress-sensitive, with core permeability decreasing as effective pressure increases. An exponential fitting function can effectively reflect the relationship between permeability and effective stress of tight sandstone cores in this area. As the air-measured permeability of the core increases, the start-up pressure gradient first decreases sharply and then gradually stabilizes. The oil–water two-phase start-up pressure gradient and permeability have a power relationship: $G = 5.66 \times 10^{-4}\ K^{-1.42}$. For tight cores, a slight increase in permeability can significantly reduce the start-up pressure gradient. This study provides a theoretical basis and technical support for the efficient development of tight oil reservoirs from a nonlinear engineering perspective, which helps to optimize development strategies and provide ideas to enhance tight oil reservoir recovery.

Keywords: tight oil reservoir, reservoir characteristics, permeability

*** Corresponding author: Xinfang Ma,** China University of Petroleum (Beijing), Beijing, 100000, China, e-mail: 17726687979@189.cn
Guodong Zeng, **Yuehao Liu:** Army Logistics Academy, Chongqing, 400000, China

1 Introduction

Unconventional oil and gas resources account for about 80% of newly explored and developed resources and have become an important part of oil and gas production. China has abundant unconventional oil and gas resources, including shale gas, tight oil, and tight gas, with broad development prospects.

Tight oil is a type of unconventional oil and gas resource, generally referring to sandstone, limestone, and other oil-bearing layers with matrix permeability less than or equal to 0.1 mD, usually with light oil quality [1]. Due to the complex pore structure and nano-scale pores in tight oil reservoirs, the fluid migration in these reservoirs differs significantly from that in conventional sandstone reservoirs, making existing seepage theories inadequate for accurate characterization and description.

X-ray diffraction (XRD) analysis shows that tight reservoirs contain various rock-forming minerals, such as quartz, calcite, dolomite, feldspar, and clay minerals [2]. With the introduction of advanced testing technologies, our understanding of tight reservoirs' microscopic pore-throat structures has deepened. Pore connectivity is a key indicator for revealing pore-throat network and connectivity structure characteristics [3]. Scholars both domestically and internationally have studied the microscopic pore-throat structure characteristics of reservoirs, focusing on pore-throat size, shape, distribution, and connectivity [4]. Tan classified pores into large and small categories using high-pressure mercury injection data [5]. Mu *et al.* used cast thin sections, scanning electron microscopy, and high-pressure mercury injection technology with fractal theory to quantitatively characterize tight sandstone pore-throat structures [6]. Tight oil reservoirs are highly heterogeneous, with poor porosity and permeability. Conventional oil reservoir technologies for improving oil-displacement efficiency are less effective in tight oil reservoirs and cannot mobilize crude oil in nano-pore-dominated tight oil reservoirs [7]. Kang *et al.* pointed out that a key reason for the difficulty in developing tight oil reservoirs is their low reservoir rock

permeability, small porosity, high capillary pressure, and poor reservoir fluid movability [8].

China has a large volume of tight oil resources, but their exploration and development are challenging and require special technologies. To enhance oil well productivity, it is crucial to study the physical property distribution and fluid seepage characteristics of tight oil reservoirs. This article explores the pore-throat characteristics and seepage features of tight oil reservoirs through lab experiments, studies seepage laws of tight reservoirs, offers data for development strategies, and helps enhance tight oil recovery.

2 Experimental methods

2.1 Material selection

Cores from the Chang-7 tight sandstone were prepared into Φ2.5 cm × H5 cm standards and cleaned with toluene, petroleum ether, and ethylene glycol, then dried [9]. Their lithological, pore-throat, and porosity–permeability characteristics were analyzed using X-ray diffraction, scanning electron microscopy, high-pressure mercury injection, permeability measurement, and porosity measurement [10].

2.2 Experimental scheme

2.2.1 Lithological characteristics

X-ray diffraction experiments were conducted to analyze the mineral composition of the Chang-7 tight sandstone. A powder sample of less than 100 mesh was prepared by crushing and sieving rock blocks, then tested with an X-ray diffractometer equipped with array detectors and scintillation counters.

Standard experimental cores of Φ2.5 cm × H5 cm were prepared from the Chang-7 tight sandstone. Rock blocks corresponding to the core were cut and crushed into 10–30-mesh particles using a geological hammer. A press was then used to further crush the particles, after which a 100-mesh sieve was employed to collect powders larger than 100 mesh for XRD testing.

2.2.2 Pore-throat characteristics

A Quanta 200 F field-emission environmental scanning electron microscope was used to observe pore-throat types and fracture shapes in rock samples. With a resolution of 1.2 nm and a magnification range of 25–200 K, it can analyze pore structures and measure pore sizes. Following the instrument's requirements, tight-reservoir cores were processed into thin sections for analysis.

One main way to study reservoir pore-throat structures in the lab is mercury injection porosimetry [11]. The capillary pressure curves from mercury injection experiments on cores can offer lots of information on the pore structures of porous media. Using relevant capillary pressure formulas, each capillary pressure value can be converted into a pore-throat radius value. The shape of the capillary pressure curve is affected by sorting and skewness, so it can also be used to analyze the pore-throat characteristics of rock samples. An automatic high-pressure mercury porosimeter was used for mercury injection experiments on several core samples from the tight reservoir to study the pore-throat distribution in the area.

2.2.3 Porosity–permeability characteristics

Porosity and permeability of sandstone samples were tested according to SY/T 5336-2006. The PDP-200 gas permeability meter was used to measure core permeability *via* the non-steady-state pulse decay method in line with the API standard. This instrument, with a measuring range of 0.00001–10 mD, ensures short experimental duration and high numerical accuracy. The KXD-3 porosity meter, based on Boyle's law and using helium as the working medium, was employed to measure the porosity of experimental cores. This method is simple to operate and offers high numerical precision. An indoor displacement device was used to measure the start-up pressure gradient of Chang-7 tight sandstone standard cores.

3 Pore-throat characteristics of tight oil reservoirs

3.1 Lithological characteristics

X-ray diffraction results showed that the Chang-7 tight sandstone has high clay mineral content, with small amounts of anhydrite and iron dolomite. The main mineral is quartz (29.4–35.8%), followed by plagioclase (20.5–26.7%), clay minerals (18.5–31.4%), and calcite (6.4–14.4%) (Table 1 and Figure 1).

Table 1: Mineral composition analysis

Sample no.	Mineral types and contents (%)								Total clay minerals (%)
	Quartz	K-feldspar	Plagioclase	Calcite	Dolomite	Talc	Anhydrite	Siderite	
C1-1	34.2	3.1	21.1	9.1	1.6	—	—	1.6	29.2
C1-2	35.8	5.2	24.9	14.4	—	—	—	1	18.5
C1-3	29.4	6.4	26.7	14.4	0.9	—	—	—	22.2
C3-1	35.5	3.5	20.5	6.4	—	—	—	2.6	31.4
C3-2	30.6	4.7	24.1	13.6	1.3	—	—	—	25.7
C3-3	32.8	10.2	21.9	14.4	—	—	—	1	19.5
C10-1	33.8	7.2	20.9	12.4	1.2	—	—	2	22.5
C10-2	40.3	10.7	28.2	5.3	—	—	—	—	15.5
L7-1	49.5	8.4	25.7	3.4	—	—	—	—	13
L7-2	16.6	3.9	33.2	1.6	14.7	25	1.6	—	3.4
L10-1	16.9	3.9	32.8	—	14.8	25.7	1.4	—	4.5
L10-2	18.5	4.2	35.3	—	11.4	27	1.7	—	1.9

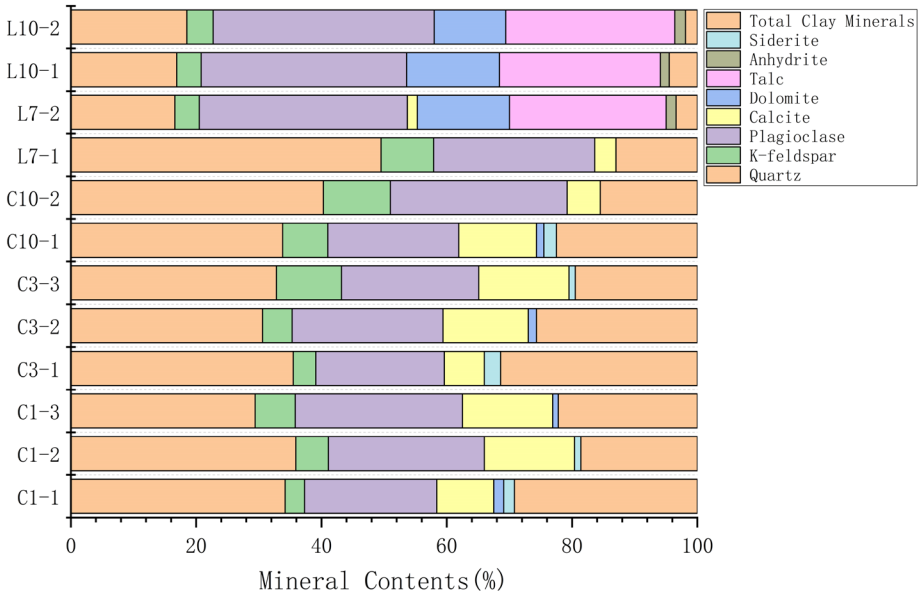

Figure 1: Composition chart of minerals.

Table 2: Clay minerals composition analysis

Sample no.	Relative content of clay minerals (%)					
	Saponite group minerals	Illite–montmorillonite mixed-layer	Illite	Kaolinite	Chlorite	Chlorite–montmorillonite mixed layers
C1-1	—	60	24	12	4	—
C3-1	—	38	42	10	10	—
C10-1	—	75	20	3	2	—
L7-1	—	20	80	—	—	—
L10-1	—	7	93	—	—	—

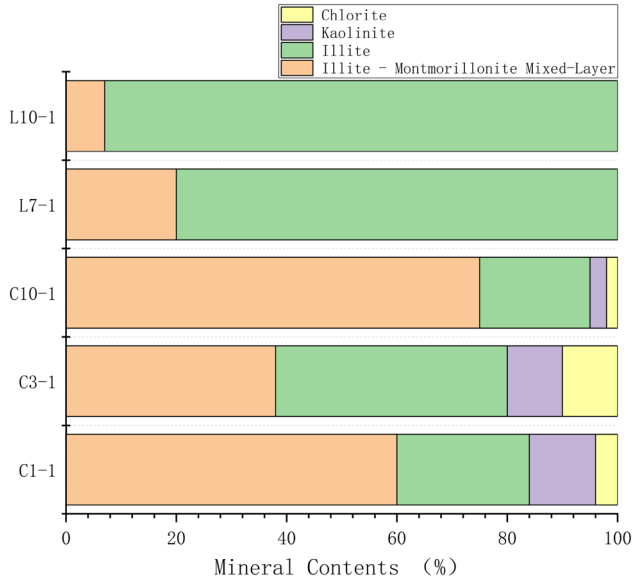

Figure 2: Composition chart of clay minerals.

As shown in Table 2 and Figure 2, the clay minerals in the Chang-7 tight cores are mainly illite–montmorillonite mixed-layers and illite, with small amounts of chlorite and kaolinite.

3.2 Pore-throat characteristics

Analysis of scanning electron microscope images indicates that the reservoir space in this area is predominantly porous with a small number of fractures. As shown in Figure 1, the pore types in the tight sandstone samples are mainly intergranular pores, intracrystalline pores, and dissolution pores. Intergranular pores, which are the primary reservoir space, have straight edges and diverse shapes (Figure 3(e)). Clay mineral intracrystalline pores, commonly formed by filamentous and flaky illite, are also prevalent and have complex shapes (Figure 3(a) and (d)). Additionally, there are dissolution micro-pores, mostly formed by feldspar dissolution, which have a honeycomb shape (Figure 3(c)). Micro-fractures, which are mostly discontinuous, are also present in the rock samples (Figure 3(b)). The presence of these irregular pore spaces and discontinuous micro-fractures significantly

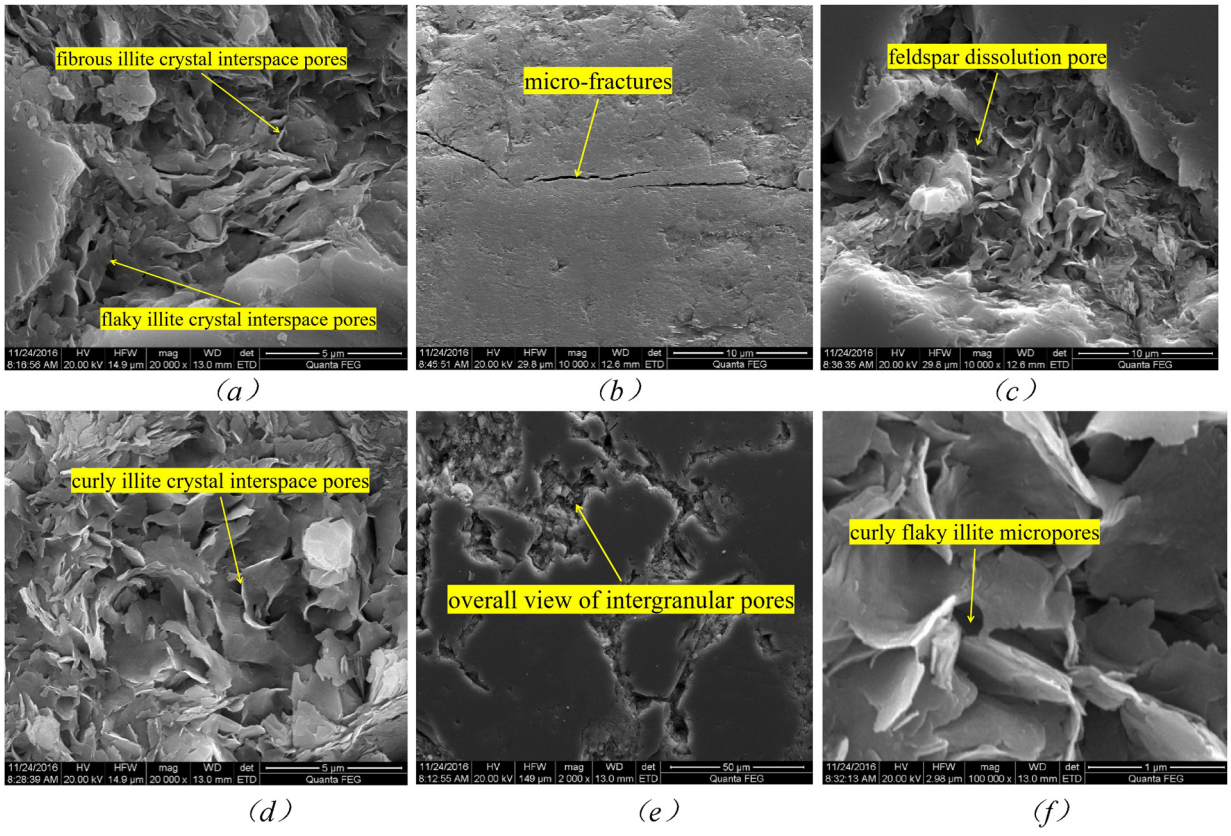

Figure 3: Pore types in tight sandstone: (a) Interspace pores of flaky and fibrous illite, C1-4; (b) micro-fractures, C1-5; (c) feldspar dissolution pore, C3-4; (d) curly illite crystal interspace pores, C3-5; (e) overall view of intergranular pores, C3-6; and (f) curly flaky illite micropores, C10 -5.

Table 3: Mercury injection parameter of core

Core sample	Permeability (mD)	Porosity (%)	Displacement pressure (MPa)	Largest pore throat radius (μm)	Average pore throat radius (μm)	Median pressure (MPa)	Median radius (μm)	Sorting coefficient	Kurtosis	Skewness	Highest mercury injection saturation (%)	Residual mercury saturation (%)	Mercury withdrawal efficiency (%)
C1	0.032	3.51	2.099	0.352	0.238	67.095	0.011	1.147	0.998	−0.364	69.57	48.71	29.99
C3	0.046	3.54	2.985	0.248	0.226	49.263	0.015	1.048	0.938	−0.175	88.74	56.69	36.13
C10	0.034	3.5	2.986	0.248	0.227	65.008	0.011	1.159	0.962	−0.334	68.99	45.81	33.61
L7	0.0028	0.35	2.989	0.248	0.155	67.736	0.011	1.606	0.582	−0.018	61.6	21.51	65.08
L10	0.003	0.34	2.993	0.247	0.186	56.103	0.013	1.548	0.635	0.285	63.07	30.46	51.7

increases the fluid flow resistance in the reservoir, resulting in the extremely low permeability of the tight sandstone.

The capillary pressure curves from mercury injection experiments on cores can offer lots of information on the pore structures of porous media. Using relevant capillary pressure formulas, each capillary pressure value can be converted into a pore-throat radius value. The shape of the capillary pressure curve is affected by sorting and skewness, so it can also be used to analyze the pore-throat characteristics of rock samples. For a particular core, if the capillary pressure curve shows good sorting and coarse skewness, it is beneficial for fluid flow. An automatic high-pressure mercury porosimeter was used for mercury injection and withdrawal experiments on each tight core to obtain the capillary pressure curves. Then, data processing was carried out to get the parameters of pore-throat size, distribution, *etc*., as shown in Table 3 and Figures 4–6.

Analysis of the pore structure characteristics of reservoir rocks from the above charts shows that the capillary pressure curves from mercury injection indicate that the core's pore throats have average sorting and are fine-grained with small radii [12]. The median radius of the tested core samples is 0.011–0.015 μm, the maximum pore-throat radius is 0.247–0.352 μm, and the average pore-throat radius is 0.155–0.238 μm. In other words, the pore-throat radii of the cores are relatively small. The maximum mercury injection saturation of the experimental core samples is 61.6–88.74%, the displacement pressure is 2.089–2.973 MPa, and the mercury withdrawal efficiency is 29.99–65.08%, indicating that the core's throats are fine and poorly connected.

In summary, the maximum pore-throat radius of the core is 0.3 μm, and the average is 0.2065 μm, with fine-grained throats. The capillary pressure curves from mercury injection of the cores show fine skewness and average sorting. The pore-throat distribution frequency and permeability contribution charts indicate that the distribution frequency and permeability contribution of pore throats do not match. There are many small throats in the cores, but they contribute little to permeability. As a result, the core's permeability is generally low, and the physical properties are poor [13].

3.3 Porosity–permeability characteristics

The porosity and permeability data of the tight cores are shown in Figure 7. Generally, porosity and permeability are positively correlated. The porosity of the cores ranges from 6 to 11% (average 8%), and permeability ranges from 0.02 to 0.08 mD (average 0.05 mD), indicating low porosity and low permeability characteristics.

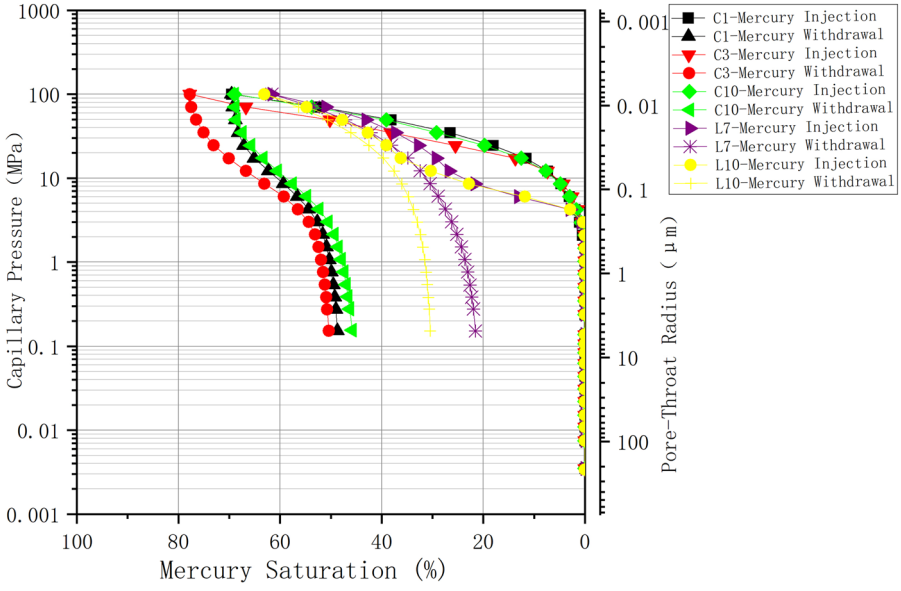

Figure 4: Mercury injection curve of core.

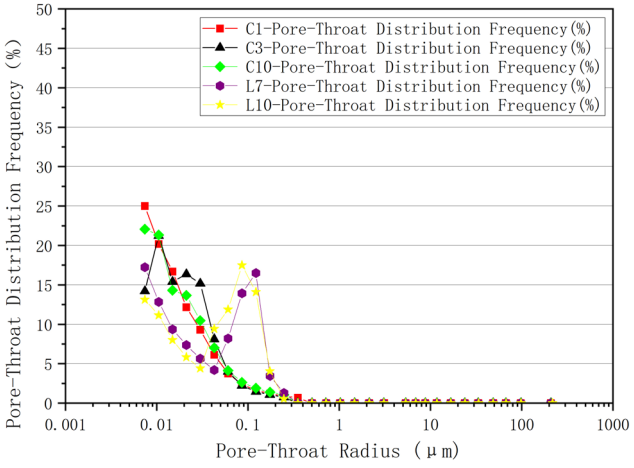

Figure 5: Pore-throat distribution frequency chart of core.

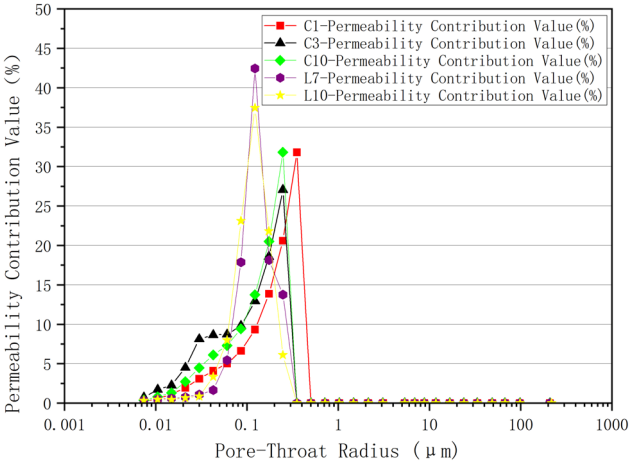

Figure 6: Permeability contribution chart of core.

An indoor displacement device was used to measure the relative permeability of tight cores, with results shown in Figure 8 and Table 4. Analysis of the Chang-7 tight core relative permeability curves shows that as water saturation increases, the relative permeability of the simulated oil declines rapidly, while that of water rises slowly. The average water saturation at the isopermeability point of the oil–water relative permeability curve is 54.5%, with an average oil–water relative permeability of 0.035 mD. The average bound water saturation of the core is 24.4%, the average residual oil saturation is 59.3%, and the average oil–water two-phase permeability interval is 34.9%. These results indicate a low amount of mobile fluid and difficult fluid flow within the experimental cores.

4 Impact of tight oil reservoir characteristics on seepage

4.1 Stress sensitivity of tight oil reservoirs

Stress sensitivity refers to the variation of reservoir rock properties with effective stress. Following the SY/T 5358-

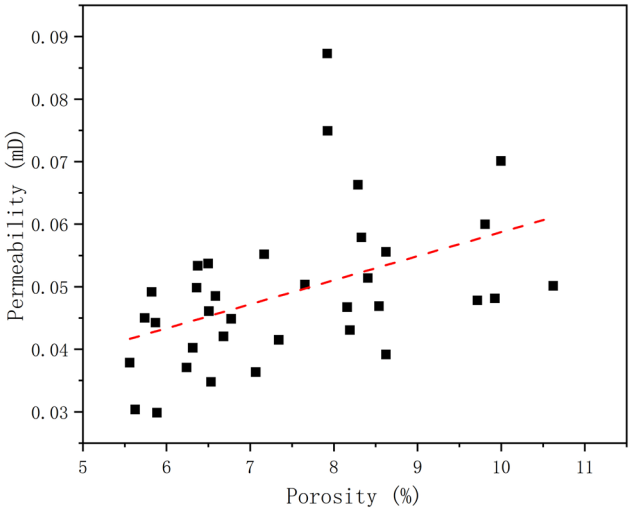

Figure 7: Relationship between porosity and permeability of tight sandstone.

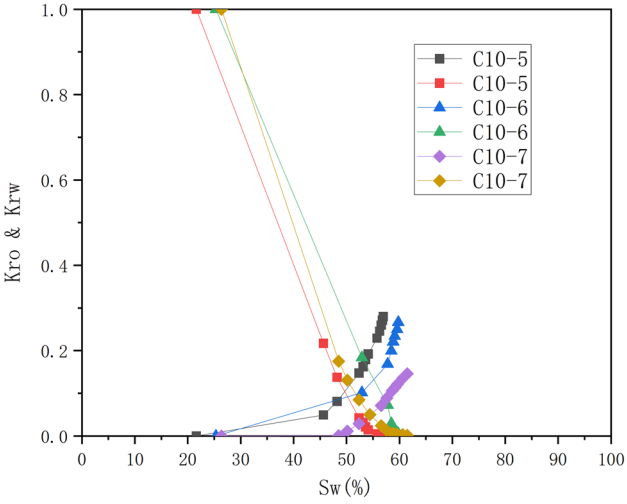

Figure 8: Relative permeability curve.

2002 standard for reservoir sensitivity flow experiment evaluation, this manuscript analyzes core stress sensitivity by changing confining pressure to measure permeability under different pressures, as shown in Table 5.

As shown in Table 5, core permeability decreases with increasing effective stress [14,15]. During pressure increase,

Table 4: Relative permeability analysis table

Formation	Permeability (mD)	Porosity (%)	Bound water		Intersection		Residual oil	
			Water saturation (%)	Oil effective permeability (mD)	Water saturation (%)	Oil–water relative permeability (mD)	Water saturation (%)	Water relative permeability (mD)
C10-5	0.19	8.7	21.6	0.0025	52.1	0.02	56.9	0.27
C10-6	0.25	9.2	25.3	0.0116	58.1	0.027	59.7	0.26
C10-7	0.29	10.3	26.3	0.0205	53.4	0.06	61.4	0.14

Table 5: Core stress sensitivity test data

Core sample		C3-1-1	C3-1-4	C3-1-19	C3-1-35
Effective stress (MPa)		Permeability (mD)	Permeability (mD)	Permeability (mD)	Permeability (mD)
Pressure increase process	4	0.021416	0.023068	0.050919	0.032051
	10	0.014869	0.016778	0.025556	0.013504
	15	0.011877	0.013413	0.014772	0.006368
	20	0.009806	0.011332	0.008947	0.003333
	25	0.007999	0.009228	0.006262	0.002146
	30	0.00667	0.007799	0.003252	0.001282
	40	0.004691	0.005712	0.001623	—
Pressure decrease process	30	0.005525	0.006757	0.002344	—
	25	0.006075	0.007519	0.003065	0.001535
	20	0.006998	0.008561	0.004553	0.002051
	15	0.008038	0.010082	0.007046	0.003156
	10	0.009751	0.012306	0.013905	0.005514
	4	0.013116	0.016906	0.027781	0.013838

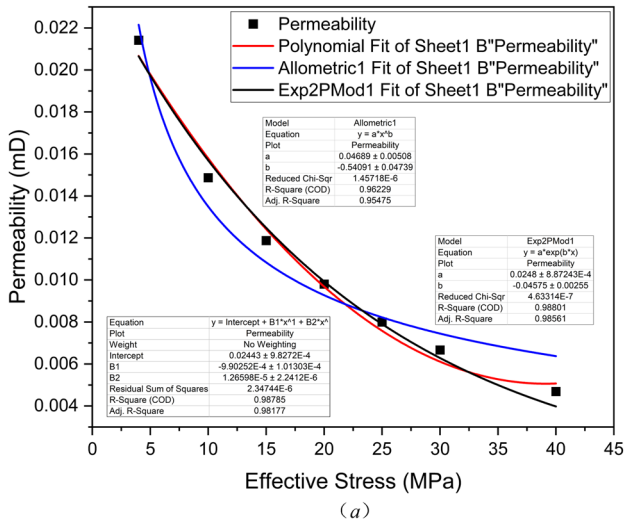

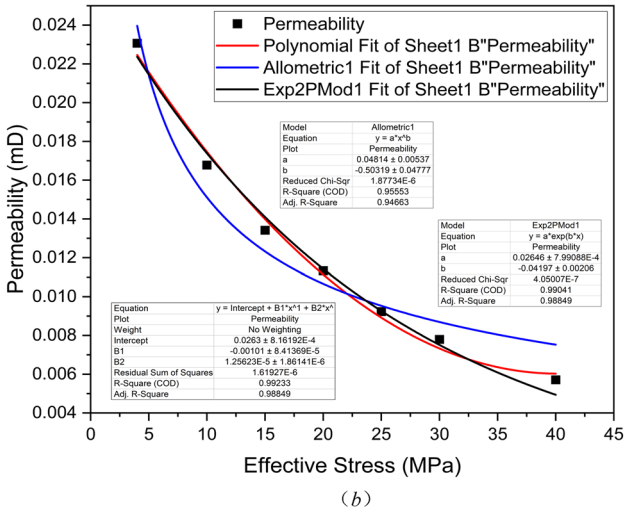

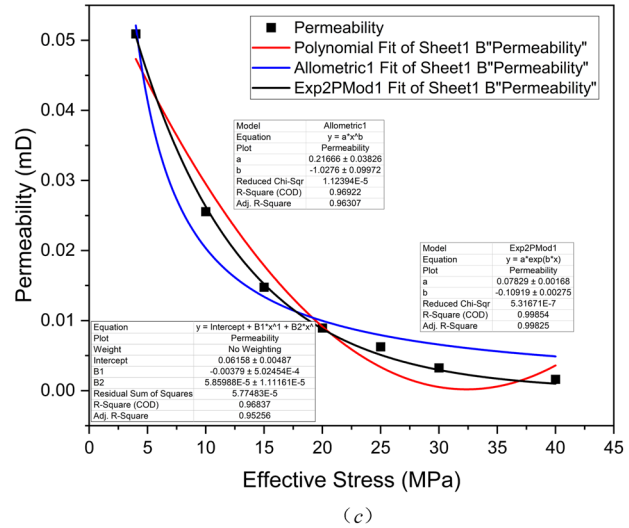

Figure 9: Fitting of stress-sensitivity data for cores during pressure increase: (a) C3-1-1, (b) C3-1-4, (c) C3-1-19, and (d) C3-1-35.

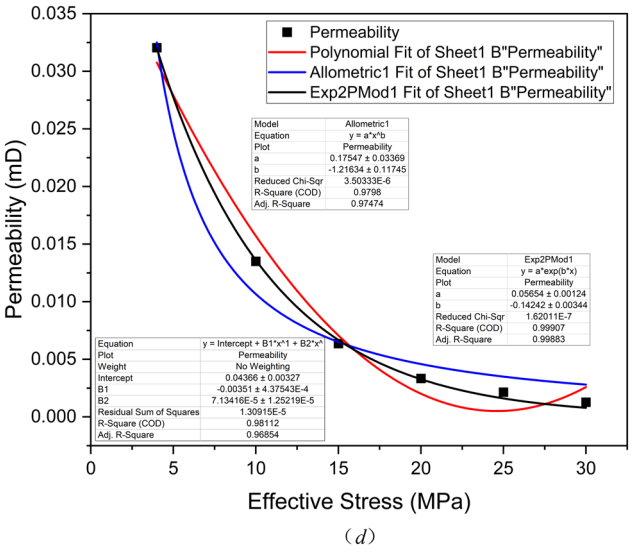

Figure 9: (*Continued*)

permeability drops rapidly at low stress and then slows down. This is because throats are compressed first and then pores as stress increases. During pressure decrease, permeability increases with reducing effective stress but remains lower than the initial value, indicating permeability damage.

To better illustrate the relationship between core permeability and effective stress, exponential, binomial, and power-law fitting were applied to the pressure-increase data of four cores, as displayed in Figure 9(a)–(d) and Table 6. Results show that the exponential fitting has the highest correlation coefficient for all four cores, indicating it can effectively reflect the stress sensitivity of permeability in tight cores in this area [16]. Thus, the exponential fitting relationship can be used in practice to represent the stress sensitivity of permeability in tight cores.

4.2 Start-up pressure gradient of tight oil reservoirs

The start-up pressure gradient of tight cores was measured using a high-precision ISCO pump, as shown in Figure 10. During the experiment, the displacement pressure difference was gradually increased at a low flow rate. Once the fluid flow stabilized, the pressure difference and flow rate data were recorded. A flow-rate *versus* pressure-gradient curve was then plotted to determine the start-up pressure gradient. In real-world oil reservoir production, during the

Table 6: Fitting of stress–permeability relationship during pressure increase for tight cores

Core	Fitting method	Regression equation	Correlation coefficient	Fitting relevance
C3-1-1	Exponential fitting	$y = 0.0248 \times 10^{-0.04575x}$	$R^2 = 0.98561$	Maximum
	Polynomial fitting	$y = 1.26598 \times 10^{-5}x^2 - 9.90252 \times 10^{-4}x + 0.02443$	$R^2 = 0.98177$	General
	Power-law fitting	$y = 0.04689x^{-0.54091}$	$R^2 = 0.95475$	Minimum
C3-1-4	Exponential fitting	$y = 0.02646 \times 10^{-0.04197x}$	$R^2 = 0.98849$	Maximum
	Polynomial fitting	$y = 1.25623 \times 10^{-5}x^2 - 0.00101x + 0.0263$	$R^2 = 0.98849$	Maximum
	Power-law fitting	$y = 0.04814x^{-0.50319}$	$R^2 = 0.94663$	Minimum
C3-1-19	Exponential fitting	$y = 0.07829 \times 10^{-0.10919x}$	$R^2 = 0.99825$	Maximum
	Polynomial fitting	$y = 5.85988 \times 10^{-5}x^2 - 0.00379x + 0.06158$	$R^2 = 0.95256$	Minimum
	Power-law fitting	$y = 0.21666x^{-1.0276}$	$R^2 = 0.96307$	General
C3-1-35	Exponential fitting	$y = 0.05654 \times 10^{-0.14242x}$	$R^2 = 0.99883$	Maximum
	Polynomial fitting	$y = 7.13416 \times 10^{-5}x^2 - 0.00351x + 0.04366$	$R^2 = 0.96854$	Minimum
	Power-law fitting	$y = 0.17547x^{-1.21634}$	$R^2 = 0.97474$	General

early stage of oil well production, formation water exists as bound water. Therefore, the oil–water two-phase start-up pressure gradient is a key indicator of the reservoir's actual mobilization status [17]. To determine this, we conduct indoor experiments to measure the oil–water two-phase start-up pressure gradient. In the experiment, simulated oil is used to displace formation water in the core, determining the bound water saturation. Then, simulated formation water is slowly injected into the core. Once the flow stabilizes, pressure and flow rate data are recorded to plot the seepage curve. The resulting start-up pressure gradient from this curve represents the core's oil–water two-phase start-up pressure gradient [18].

As shown in Figure 11, which illustrates the oil–water two-phase start-up pressure gradient for tight cores, the gradient initially rises slowly with decreasing core permeability. Once the permeability drops below a certain threshold, the gradient escalates sharply. This occurs because tighter cores, with finer pore throats, intensify the Jamin effect and other phenomena, requiring greater pressure for fluid flow. Analysis reveals a power-law relationship between the start-up pressure gradient and permeability: $G = 5.66 \times 10^{-4}\ K^{-1.42}$. For instance, when the permeability of a tight core is 0.02 mD, the oil–water two-phase start-up pressure gradient is approximately 0.153 MPa/cm. However, when the core's permeability increases to 0.2 mD, this gradient drops to 0.0084 MPa/cm, highlighting the significant impact of permeability changes on reservoir development [19].

4.3 Dynamic capillary force in tight oil reservoirs

In tight sandstone reservoirs, poor rock properties and small pore throats result in high oil–water capillary forces.

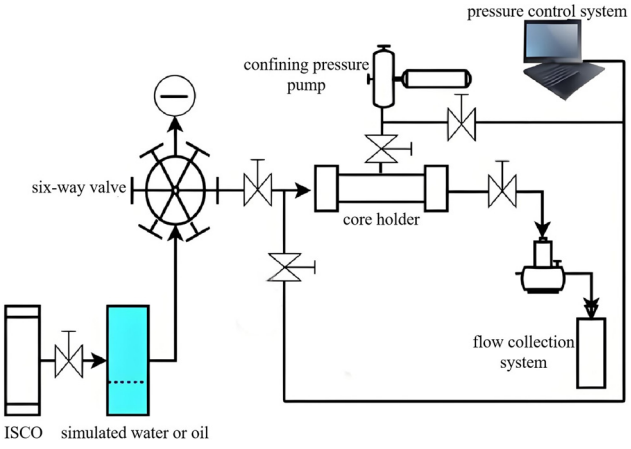

Figure 10: Schematic diagram of start-up pressure gradient measurement device.

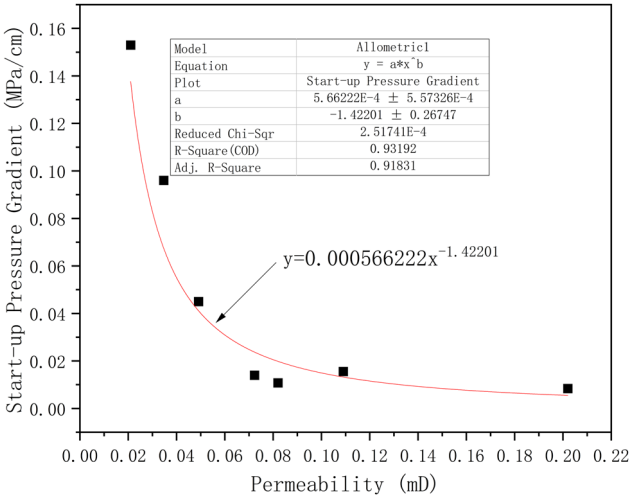

Figure 11: Fitting curve of oil–water two-phase start-up pressure gradient for tight cores.

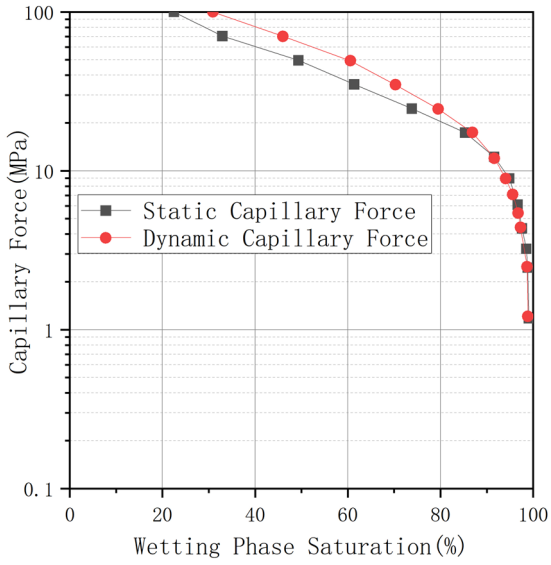

Figure 12: Dynamic and static capillary force curves of Core C10.

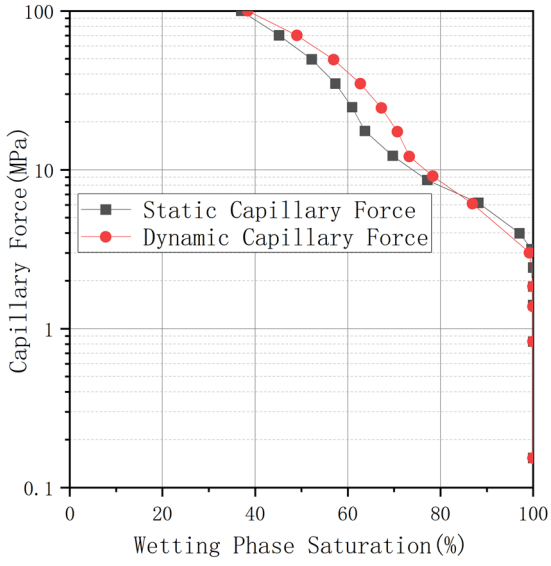

Figure 13: Dynamic and static capillary force curves of Core L10.

During development, fluids in the reservoir are usually in an unstable state, leading to differences between the interfacial capillary forces of oil–water two-phase flow and conventional static capillary forces. This is known as the dynamic capillary force effect, which can impact fluid seepage and, consequently, oil well productivity [20,21].

The most commonly used formula for dynamic capillary force in oil–water two-phase seepage was derived by Hassanizadeh and Gray [22]. The formula is as follows:

$$P^{\mathrm{dyn}} - P^{\mathrm{equ}} = -\tau \frac{\partial S_{\mathrm{w}}}{\partial t}$$

where P^{dyn} and P^{equ} are the dynamic and static capillary forces (in MPa), S_{w} is the wetting phase fluid saturation (a decimal), and τ is the non-equilibrium capillary force coefficient, typically obtained through experimental measurement.

An automatic mercury porosimeter was used to measure the capillary force of tight cores. When the equilibrium time for fast mercury injection was 10–50 s, the two-phase interface did not reach equilibrium, resulting in strong dynamic effects and a dynamic capillary force curve. For an equilibrium time of 300–600 s, a static capillary force curve was obtained.

As shown in Figures 12 and 13, the dynamic and static capillary forces for two cores at the same saturation level differed by up to 27.3 and 45.1%. This indicates a significant difference between dynamic and static capillary forces, which must be considered in tight oil reservoir development.

5 Conclusions

This manuscript presented an experimental study on Chang-7 tight sandstone. The following conclusions can be drawn from this study:

(1) The Chang-7 tight sandstone cores consist mainly of quartz arenite and feldspar arenite with high clay mineral content. The pore types are predominantly intergranular pores, clay mineral intercrystalline pores, dissolved pores, and micro-fractures. The average porosity is 8%, and average permeability is 0.05 mD, with a general positive correlation between porosity and permeability. The small oil–water two-phase permeability interval indicates difficult fluid flow in the cores.

(2) The tight cores exhibit stress sensitivity, with permeability decreasing as effective pressure increases. During initial pressure increase, permeability drops rapidly and then slows down. Exponential fitting best describes the relationship between permeability and effective stress.

(3) The start-up pressure gradients of tight cores with different permeabilities were measured experimentally. The start-up pressure gradient decreases sharply with increasing core permeability and then stabilizes. The oil–water two-phase start-up pressure gradient and permeability follow a power relationship: $G = 5.66 \times 10^{-4}\ K^{-1.42}$. Even a slight increase in permeability can significantly reduce the start-up pressure gradient in tight cores.

(4) Dynamic capillary force measurements show significant differences from static capillary force, indicating the need to consider dynamic capillary force effects in tight oil reservoir development.

Next, an oil-well productivity prediction model for tight oil reservoirs will be established using this study's experimental data and results. The model will incorporate stress sensitivity, start-up pressure gradient, and dynamic capillary force of tight oil reservoirs to provide accurate productivity prediction and help enhance tight oil recovery.

Funding information: Authors state no funding involved.

Author contributions: Conceptualization: Guodong Zeng, Xinfang Ma, and Yuehao Liu; methodology: Guodong Zeng; conduct experiments: Guodong Zeng and Yuehao Liu; analyze experimental data: Guodong Zeng, Xinfang Ma, and Yuehao Liu; writing – original draft preparation: Guodong Zeng and Yuehao Liu; writing – review and editing: Xinfang Ma; supervision: Yuehao Liu; project administration: Xinfang Ma. All authors have accepted responsibility for the entire content of this manuscript and approved its submission.

Conflict of interest: Authors state no conflict of interest.

Data availability statement: The datasets generated during and/or analyzed during the current study are available from the corresponding author on reasonable request.

References

[1] Nilsson C, Raun K, Yan F, Larsen MO, Tang-Christensen M. Types, characteristics, genesis and prospects of conventional and unconventional hydrocarbon accumulations: taking tight oil and tight gas in China as an instance. Acta Petrol Sin. 2012;33(2):173–87.

[2] Wu S, Zhu R, Yang Z, Mao Z, Cui J, Zhang X. Distribution and characteristics of lacustrine tight oil reservoirs in China. J Asian Earth Sci. 2019;178:20–36.

[3] Zhao J, Hu Q, Liu K, Jin Z, Dultz S, Kaufmann J, et al. Pore connectivity characterization of shale using integrated wood's metal impregnation, microscopy, tomography, tracer mapping and porosimetry. Fuel. 2020;259:116248.

[4] Qu HJ, Yang B, Tian XH, Liu XS, Yang H, Dong WW, et al. The primary controlling parameters of porosity, permeability, and seepage capability of tight gas reservoirs: a case study on Upper Paleozoic Formation in the eastern Ordos Basin, Northern China. Pet Sci. 2019;16:1270–84.

[5] Tan Q, Kang Y, You L, Xu F, Meng S. A comprehensive insight into the multiscale pore structure characterization of saline-lacustrine tight carbonate reservoir. J Pet Sci Eng. 2020;187:106744.

[6] Mu C, Hua H, Wang X. Characterization of pore structure and reservoir properties of tight sandstone with CTS, SEM, and HPMI: a case study of the tight oil reservoir in fuyu oil layers of Sanzhao Sag, Songliao basin, NE China. Front Energy Res. 2023;10:1053919.

[7] Van Wagener D, Aloulou F. Tight oil development will continue to drive future US crude oil production. United States: US Energy information administration. Vol. 28, 2019.

[8] Kang Y, Tian J, Luo P, You L, Liu. X. Technical bottlenecks and development strategies of enhancing recovery for tight oil reservoirs. Acta Petrol Sin. 2020;41(4):467–77.

[9] Chao Z, Xiaohan Q, Aifang Z, Shinian C, Haibin G, Jin W, et al. Microscopic pore structure of tight sandstone reservoirs and its influence on oil–water seepage. J Xi'an Shiyou Univ. 2024;39:65–73+84.

[10] Jie C, Ying ZG, Liang ZX, Cheng H. Overview of study methods of reservoir rock pore structure. Spec Oil Gas Reservoirs. 2005;12(4):11–4.

[11] He S, Jiao C, Wang J, Luo F, Zou L. Discussion on the differences between constant-speed mercury injection and conventional mercury injection techniques. Fault-Block Oil Gas Field. 2011;18(2):235–7.

[12] Jiyong Z, Zhenwang L, Qichao X, Jingping Z. Micro pore throat structural classification of Chang 7 tight oil reservoir of Jiyuan Oilfield in Ordos Basin. China Pet Exploration. 2014;19(5):73–9.

[13] Li ZQ, Fan YR. Pore-throat distribution of carbonate reservoir in Tahe oilfield. West-China Explor Eng. 2010;22(11):138–40.

[14] Rong NX, Long WC, Jiao L. Experimental study on stress sensitivity for tight reservoirs based on time scale. Unconv Oil Gas. 2016;3(4):21–4.

[15] Wei SY, Fang CY, Fang ZW, Xia SF, Ming YS. Analysis of stress sensitivity and optimization of fracturing parameter for tight reservoirs. Fault-Block Oil Gas Field. 2018;25(4):493–7.

[16] Xi Z, YuMing S, ChengYun H, Jingmei G. Experimental research and analysis on stress-sensitive of low permeability reservoir sandstone. Xinjiang Oil Gas. 2011;07(1):76–80.

[17] Zhu WY, Tian W, Zhu HY, Zhang XL, He YQ, Li Y, et al. Study on experiment of threshold pressure gradient for tight sandstone. Sci Technol Eng. 2015;15(3):79–83.

[18] Zheng MQ, Lai YS, Ping LD, Gen K, Hao L, Can C. Study on the physical properties of tight reservoir and the regularity of the threshold pressure gradident—taking the Xinjiang Jimsar Basin Lucaogou Group as an example. Sci Technol Eng. 2016;16(24):42–7.

[19] Yongchao X, Xiaofeng T. Characteristics of Chang-7 tight oil, Ordos basin. Spec Oil Gas Reservoirs. 2014;21(3):111–5.

[20] Wang JC, Zhang WY, Zhong Z, Wei AB, Bao QH, Zhang Y, et al. Dynamic effect of capillary pressure in low permeability reservoirs. Pet Explor Dev. 2012;39(3):378–84.

[21] Yong ZH, Li HS, Yan JC, Quan MC, Hua LG, Yuan MS, et al. Study of dynamic capillary pressure in ultra-low permeability reservoir. Sci Technol Eng. 2013;13(12):3261–6.

[22] Hassanizadeh SM, Gray WG. Mechanics and thermodynamics of multiphase flow in porous media including interphase boundaries. Adv Water Resour. 1990;13(4):169–86.